09

Synthesis and Testing of $BaZrGe_3O_9:Mn^{4+}$ for Application as a Red-Emitting Phosphor

© X. Wang[1], M. Zhai[1], K.V. Ivanovskikh[2], H. Guo[1], P. Huang[1], C. Cui[1], L. Wang[1], Q. Shi[1,¶],

[1] College of Physics and Optoelectronics, Taiyuan University of Technology, Taiyuan, 030024 China
[2] Department of Experimental Physics, Ural Federal University, Ekaterinburg, 620002 Russia

¶ E-mail: shiqiufeng@tyut.edu.cn

Received June 16, 2022
Revised June 16, 2022
Accepted June 19, 2022

A series of novel red-emitting phosphors $BaZrGe_3O_9:Mn^{4+}$ ($BZG:Mn^{4+}$) were synthesized through high-temperature solid-state reaction method in order to explore their capabilities for application as red-emitting phosphors. The phosphors were characterized by X-ray diffraction, photoluminescence spectra, and decay curve measurements at the temperature ranging from 80 to 500 K. The luminescence intensity increases to maximum at doping concentration of 0.2 mol.%, and then decreases with concentration. Serious thermal quenching was also revealed.

Keywords: red-emitting phosphor, germanate, Mn^{4+}, concentration quenching, thermal stability.

1. Introduction

White light-emitting diodes (WLEDs) attract considerable attention of researchers worldwide due to their excellent performance in terms of durability, long lifetime, and energy-saving effects which obviously result in many economic benefits from their extensively expanding use. Commercial phosphor-converted WLEDs (pc-WLEDs) are composed of blue-emitting InGaN chip and green/yellow-emitting and orange/red-emitting phosphors that convert part of the blue InGaN emission. Deficiency of the red spectral component is a well-known problem for $YAG:Ce^{3+}$-based WLEDs that limits their applications for indoor lighting requiring warmer light. Another method is based on combining near-UV GaN or AlGaN chips with green, blue, and red phosphors. Since recently, extensive research has been conducted for the development of novel luminescent materials suitable for application as red emitting phosphors in pc-WLED. Among them, Mn^{4+}-doped materials were proposed to demonstrate better luminous efficacy, higher colour rendering index and low colour temperature (< 4000 K) [1–5].

The electronic configuration of transition metal ion Mn^{4+} is $3d^3$, energy levels of which in an octahedral crystal field (assuming Racah parameters being $C = 4.5$ B) could be obtained according to the Tanabe–Sugano energy-level diagram [6]. The excitation transitions involved are from ground state $^4A_2$ to excited states $^4T_1$ and $^4T_2$, respectively. Due to the strong influence on $^4T_1$ and $^4T_2$ by the crystal field splitting, these excitations are characterized by broad absorption bands. The emission transition originates from ^2E_g to $^4A_2$ and is characterized by line emissions, which is attributed to the ^2E_g state independence of crystal field splitting. Owing to the fact of parity forbidden and spin forbidden for $^2E_g \rightarrow {}^4A_2$ transition, the lifetime of the corresponding ^2E_g emission is of order of milliseconds [7].

Photoluminescence quantum efficiencies (QEs) is a very important parameter for phosphors. Temperature and concentration quenching are among the factors affecting the QEs, especially for Mn^{4+}-activated phosphors. The energy level structure of Mn^{4+} in a specific host lattice determines the quenching temperature, while the mechanism of quenching generally occurs through thermally activated crossover between excited state and ground state [8,9]. In addition, an anomalous thermal quenching behaviour was observed to increase integrated photoluminescence intensity with T increasing in a temperature range. Also possible mechanisms responsible for this phenomenon were proposed but they still remain debatable [10–13]. As mentioned above, Mn^{4+} 3d–3d transition is parity-forbidden. To increase absorption efficiency of blue light from LED chip, a higher doping concentration can be a solution. However, the quenching concentration is very low for Mn^{4+}-activated hosts and the related mechanism is still an open question. Therefore, the study on photoluminescence properties of Mn^{4+}-activated inorganic materials is not only of interest for understanding the mechanisms of thermal and concentration quenching, but also helpful for the development of novel red or far red Mn^{4+}-activated phosphors.

While searching for new inorganic hosts suitable for doping with Mn^{4+} ions, we found it inspiring to test $BaZrGe_3O_9$ (BZG) that, being a representative of the germanate family, is expected to have good thermal stability and moisture resistance. Recently, quite promising results were obtained for $Y_2Mg_3Ge_3O_{12}:Mn^{4+}$, Li^+ [14] that

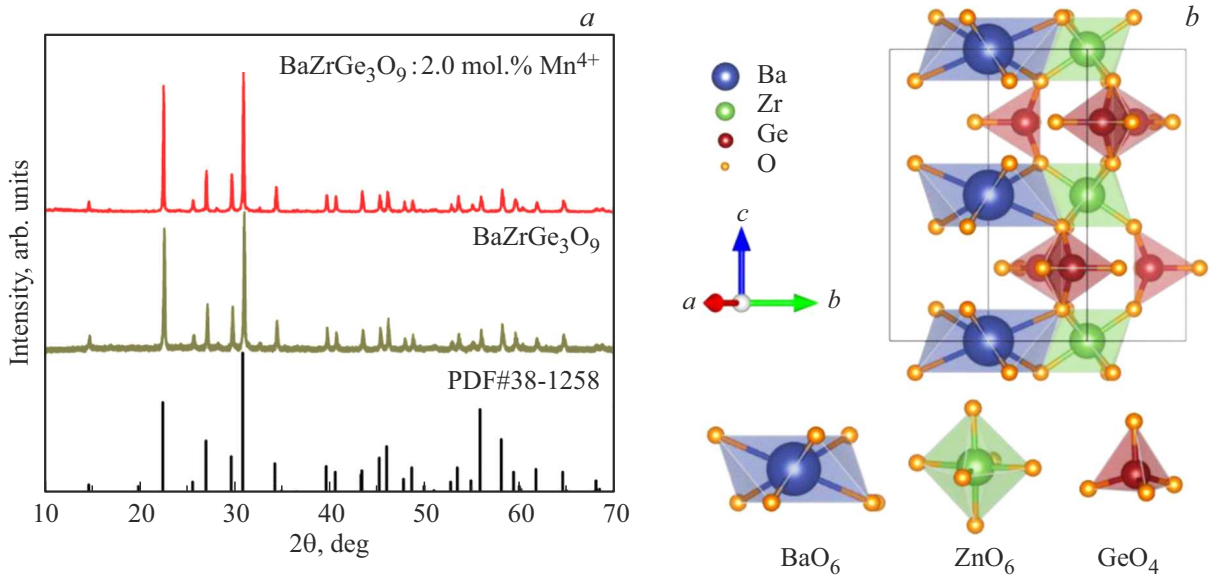

Figure 1. *a*) XRD patterns of non-doped BZG and BZG : 2.0 mol.% Mn^{4+} samples confronted with the standard XRD pattern (PDF #38-1258), *b*) crystal structure of host lattice BZG.

demonstrated high thermal quenching temperature for deep red Mn^{4+} emission. As for BZG host, it was reported to demonstrate excellent photoluminescence properties when doped with Eu^{3+} [15], Pr^{3+} [16], and Cr^{3+} [17,18]. The crystal structure of this host suggests that Zr^{4+} is coordinated with six O^{2-} ions forming octahedral structure, which is a favourable environment for Mn^{4+} ion.

In this work, we investigate the photoluminescence properties including concentration quenching and thermal quenching of Mn^{4+}-doped BZG. Photoluminescence spectra and decay curves of BZG : *x* mol.% Mn^{4+} ($x = 0.1-2.0$) are studied in the temperature range from 80 to 550 K. BZG : 0.2 mol.% with deep red luminescence at around 667 nm processes the maximum intensity, which may have potential application in pc-WLED for indoor plant cultivation. The results obtained in this study are also beneficial for better understanding of concentration and thermal quenching in Mn^{4+}-activated phosphors.

2. Experiments

A series of BZG : x mol.% Mn^{4+} ($x = 0.1-2.0$) were prepared following a solid-state reaction method [15], using $BaCO_3$ (analytical reagent grade, A.R.), ZrO_2 (A.R.), GeO_2 (99.99%), and MnO_2 (A.R.) as raw materials. Stoichiometric amounts of raw materials were weighed and homogeneously ground in an agate mortar. The mixtures were calcined in corundum crucibles at 1200° for 4 h and naturally cooled down to room temperature (RT). The final products were ground once again for further characterization.

Powder X-ray diffraction (XRD) patterns over the range from 10 to 80° were collected using a Shimadzu XRD-6000 diffractometer equipped with a Cu target (Kα, $\lambda = 1.5405$ Å) as an X-ray source operating at 40 kV and 30 mA. Photoluminescence spectra and decay curves measurements were performed on an Edinburgh Instrument FLS1000 spectrometer upon excitation with an ozone-free Xenon arc lamp (450 W, 230–1000 nm) and a microsecond flash lamp (μF_2, pulse width 1–2 μs), respectively. A cooled (−20°) single-photon counting photomultiplier tube (Hamamatsu R928P, working range 200–900 nm) was used as a detector for both photoluminescence spectra and decay curves measurements. The temperature of samples was controlled by an Oxford Instruments Microstat N2 cryostat (working range 80–300 K) and a Techcomp heating stage (300–550 K).

3. Results and discussion

3.1. XRD patterns and crystal structure

XRD patterns of undoped and maximum 2.0% Mn^{4+}-doped BZG samples as most representative are shown along with the standard XRD pattern of PDF card #38-1258 in Fig. 1, *a*. XRD patterns of intermediate doped samples are not shown for brevity. The position of diffraction peaks agrees well with that of the standard pattern, while no extra peaks appear indicating successful synthesis of hexagonal BZG phase. In addition, the position of diffraction peaks of the sample with maximum concentration at 2.0 mol.% Mn^{4+} in this work does not shift revealing that the dopant almost has no effect on the crystal structure parameters. The crystal system of the BZG host lattice is hexagonal with space group of P6c2 (188) as shown in Fig. 1, *b*. The cations coordination environments are also demonstrated in Fig. 1, *b*. It can be seen that both Ba^{2+} and Zr^{4+} are

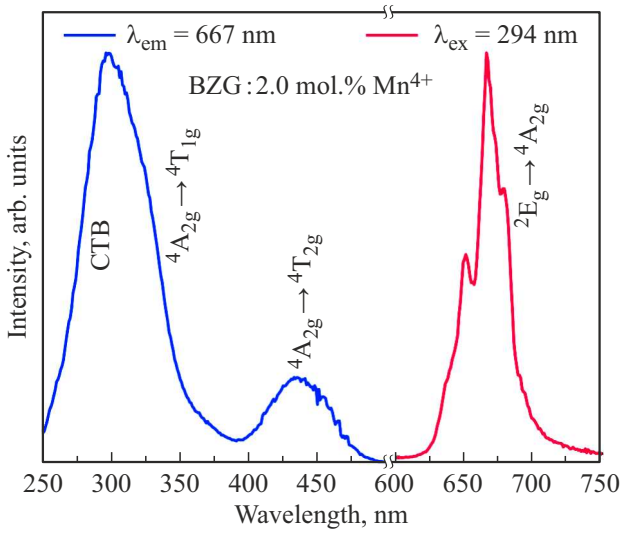

Figure 2. Excitation spectrum (on the left) recorded monitoring Mn^{4+} emission at 667 nm, and emission spectrum (on the right) recorded upon excitation at 294 nm for BZG:0.2 mol.% Mn^{4+} at RT.

coordinated with six oxygen anions forming polyhedron and octahedron, respectively. Ge^{4+} is coordinated with four oxygen forming tetrahedron. Considering the fact of same valence state and similar effective ionic radii between Zr^{4+} (0.72 Å for CN = 6) and Mn^{4+} (0.53 Å for CN = 6) ions, that latter are supposed to occupy Zr^{4+} sites [19].

3.2. Photoluminescence properties

The excitation and emission spectra of BZG:0.2 mol.% Mn^{4+} recorded at RT are demonstrated in Fig. 2. The excitation spectrum (on the left) is obtained by monitoring the emission connected with Mn^{4+} $^2E_g \rightarrow {}^4A_{2g}$ transition at 667 nm. The excitation spectrum is composed of two broad excitation bands centred near 435 and 294 nm which originate from Mn^{4+} spin-allowed intraconfigurational $^4A_{2g} \rightarrow {}^4T_{2g}$ and $^4A_{2g} \rightarrow {}^4T_{1g}$ transitions in octahedral coordination, respectively, as indicated in Fig. 2. A higher relative intensity of the short wavelength excitation is explained by superposition with an $O^{2-}-Mn^{4+}$ charge transfer band (CTB) that is situated at around 280 nm with an energy little higher than Mn^{4+} $^4A_{2g} \rightarrow {}^4T_{1g}$ transition. Similar $O^{2-}-Mn^{4+}$ CTB was earlier documented to be observed in $Y_2Mg_3Ge_3O_{12}:Mn^{4+}$, Li^+ [14].

The emission spectrum recorded upon intraconfigurational $^4A_{2g} \rightarrow {}^4T_{1g}$ excitation at 294 nm (Fig. 2, on the right) is dominated by a group of superimposed emission features with most pronounced one peaked at $\sim$ 667 nm which are attributed to Stokes and anti-Stokes Mn^{4+} $^2E_g \rightarrow {}^4A_{2g}$ transitions [20].

The concentration-dependent emission spectra and decay curves of BZG:x mol.% Mn^{4+} recorded upon $^4A_{2g} \rightarrow {}^4T_{1g}$ excitation at 294 nm at RT are shown in Fig. 3. As it can be seen from the spectra, a maximum intensity is observed for the sample doped 0.2% of Mn^{4+} while further increase of the doping concentration leads to gradual drop of emission intensity. The initial rise of emission intensity with

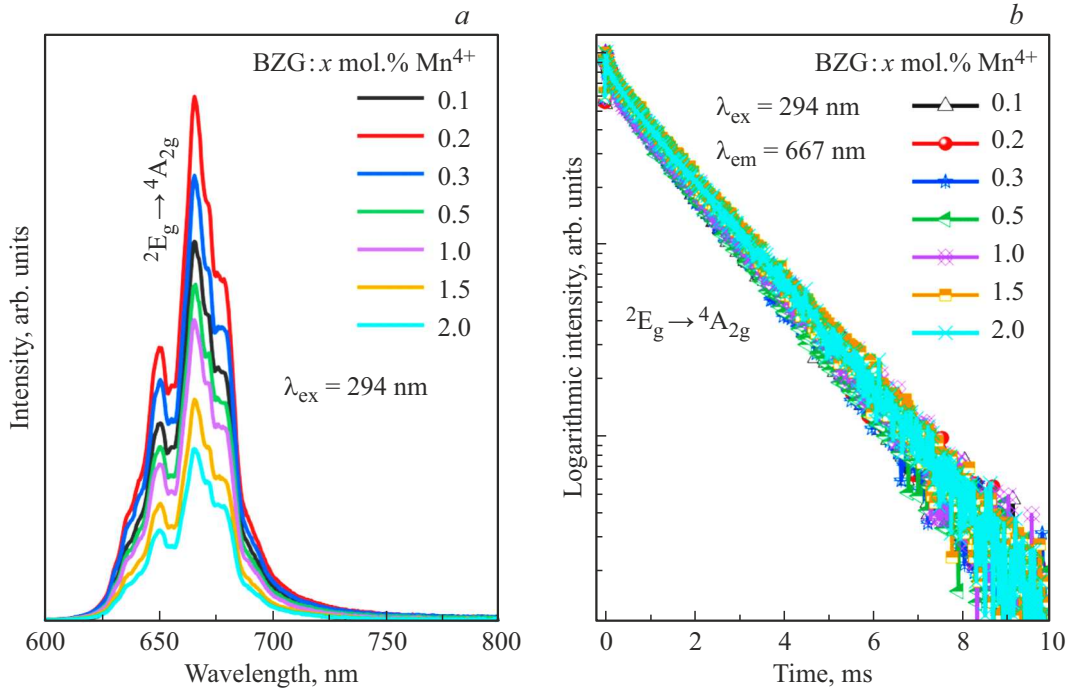

Figure 3. Mn^{4+} concentration-dependent *a*) emission spectra and *b*) $^2E_g \rightarrow {}^4A_{2g}$ emission decay curves of BZG:x mol.% Mn^{4+} (x = 0.1, 0.2, 0.3, 0.5, 1.0, 1.5, and 2.0) recorded upon excitation into Mn^{4+} ^2E_g state at 294 nm at RT.

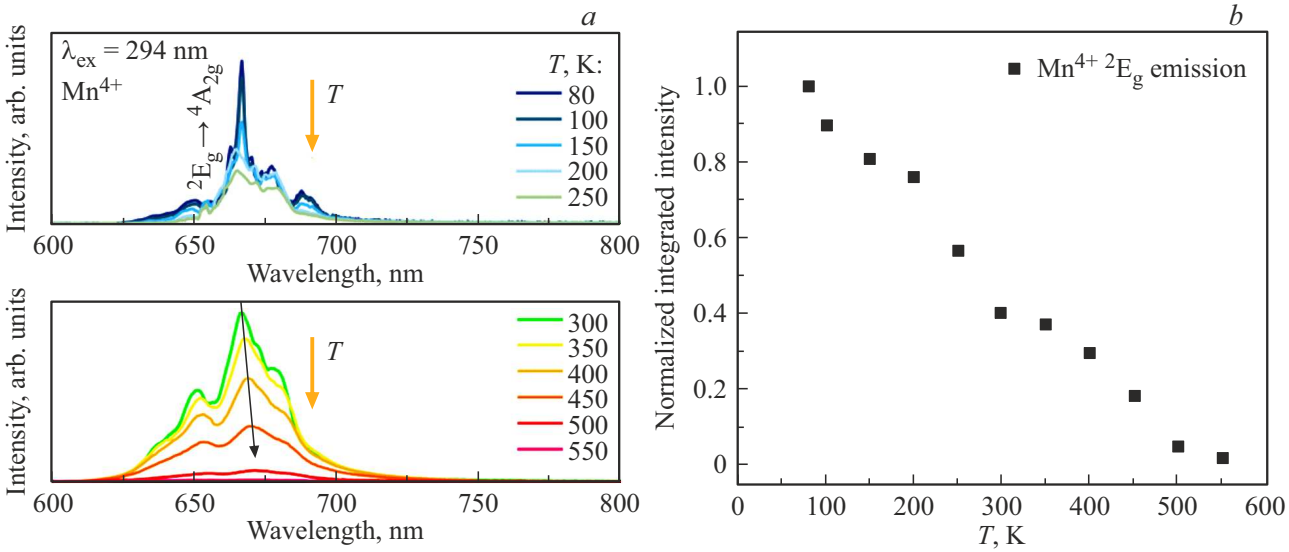

Figure 4. *a*) Temperature-dependent emission spectra and *b*) normalized temperature dependence of integrated $^2E_g \rightarrow {}^4A_{2g}$ emission intensity for BZG : 0.2 mol.% Mn^{4+} recorded upon excitation into Mn^{4+} ^2E_g state at 294 nm.

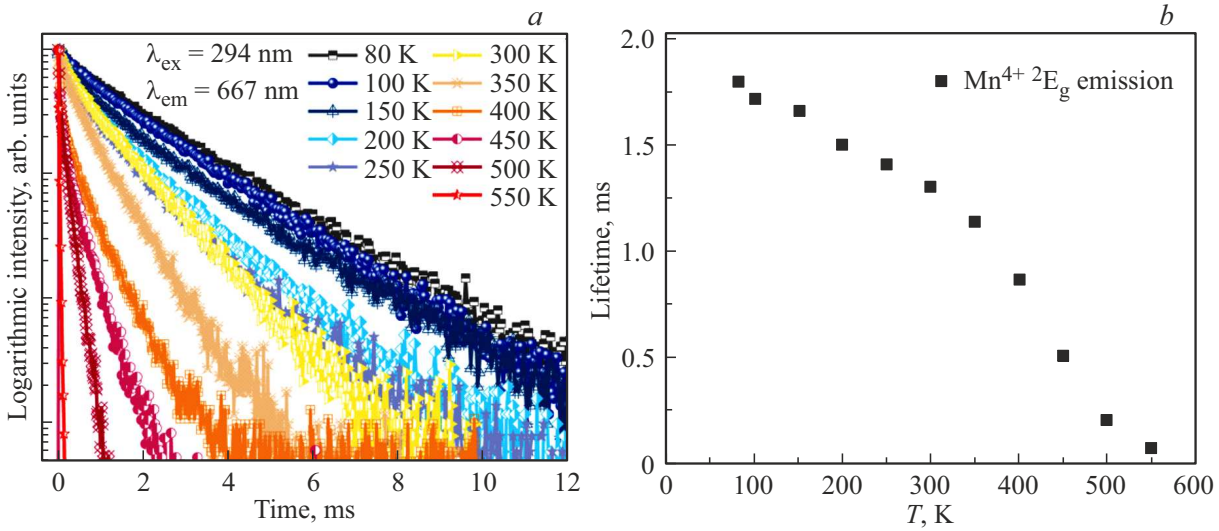

Figure 5. Temperature-dependent *a*) decay curves and *b*) decay time of Mn^{4+} ^2E_g state luminescence (BZG : 0.2 mol.% Mn^{4+}) upon excitation into Mn^{4+} ^2E_g state at 294 nm.

increasing of dopant concentration is obviously attributed to the increase of number of emitting centres. Further increase of doping concentration results in shortening of distances between Mn^{4+} ions that triggers energy migration among them and eventually promotes transfer of excitation energy to defects (killer centres). The observed concentration quenching of Mn^{4+} luminescence is supposed to be accompanied by shortening of lifetime. However, the decay curves recorded for the $^2E_g \rightarrow {}^4A_{2g}$ emission of Mn^{4+} are almost concentration independent with no obvious shortening of lifetime that keeps stable at about 1.5 ms. The same effect was observed upon $^4A_{2g} \rightarrow {}^4T_{2g}$ excitation at 435 nm (not shown for brevity). We suppose that the observed phenomenon originates from quenching of Mn^{4+} luminescence through a single-step energy transfer to neighbouring quenchers. In this case, the quenching is expected to speed up the initial (right after the excitation) stage of the decay curves with no influence on the longer time stage. The same phenomenon has been previously observed Mn^{4+} $^2E_g \rightarrow {}^4A_{2g}$ emission $K_2TiF_6:Mn^{4+}$ [8]. Unfortunately, we were not able to distinguish any acceleration of decay curves in the initial stage of the recorded decay curves because of low time resolution of the setup that was rather designed for measurements millisecond-order decay kinetics.

The emission spectra of optimally doped BZG : 0.2 mol.% Mn^{4+} phosphor in the temperature range from 80 to

550 K are presented in Fig. 4, *a*. The spectra reveal decrease of emission intensity with temperature increasing that suggest the occurrence of temperature quenching for the ^2E_g excited state. In addition, the emission peaks get broadened and shifted towards longer wavelength with temperature. The normalized temperature dependence of integrated $^2E_g \rightarrow {}^4A_{2g}$ emission intensity presented in Fig. 4, *b* shows nearly linear decrease with temperature increasing. The mechanism responsible for temperature quenching is attributed to thermal activation of electron from ^2E_g state to $^4A_{2g}$ ground state through the crossover between the Franck–Condon shifted $^4T_{2g}$ and $^4A_{2g}$ ground states [8].

Fig. 5 demonstrates the temperature-dependent decay curves of Mn^{4+} $^2E_g \rightarrow {}^4A_{2g}$ emission and temperature dependence of its average lifetime for BZG : 0.2 mol.% Mn^{4+} recorded upon $^4A_{2g} \rightarrow {}^4T_{1g}$ excitation at 294 nm. The decay curves taken at temperatures of 80 and 100 K are almost single exponential and show lifetime of about 1.7 ms. Increasing of temperature results in departure of the decay curves from single exponential behaviour. Moreover, fitting the corresponding decay curves with two exponential decay function did not lead to satisfactory results. Due to this, the decay curves recorded at 150 K and above were analysed via average lifetime as suggested in [21]. The average lifetime shows systematic decrease with temperature and gets minimum of about 0.07 ms at 550 K.

4. Conclusion

A deep red emitting BGZ : Mn^{4+} phosphor was successfully synthesized via a conventional solid state reaction. The temperature and Mn^{4+}-concentration dependencies of photoluminescence, spectroscopic, and decay properties were investigated. The optimum concentration of Mn^{4+} was found to be about 0.2 mol.%. Although the phosphor demonstrates well-pronounced deep red emission at RT, its commercial application is questionable due to significant thermal quenching originated from crossover of $^4T_{2g}$ excited state and $^4A_{2g}$ ground states.

Funding

This work was financially supported by the Key Research and Development (R&D) Projects of Shanxi Province (201903D121097) and Natural Science Foundation of Shanxi Province (20210302123127). K. Ivanovskikh acknowledges partial support by the Ministry of Science and Higher Education of the Russian Federation (Project No FEUZ-2020-0060).

Confilicts of interests

The authors declare that they have no conflicts of interest.

References

[1] W. Zhang, M. He, X. Qiao, X. Fan. Chinese J. Lumin. **42**, *9*, 1345 (2021).
[2] M.G. Brik, C. Ma, A.M. Srivastava, M. Piasecki. Chinese J. Lumin. **41**, 1011 (2020).
[3] Q. Zhou, L. Dolgov, A.M. Srivastava, L. Zhou, Z. Wang, J. Shi, M.D. Dramicanin, M.G. Brik, M. Wu. J. Mater. Chem. C **6**, *11*, 2652 (2018).
[4] T. Senden, E.J. van Harten, A. Meijerink. J. Lumin. **194**, 131 (2018).
[5] H. Zhu, C.C. Lin, W. Luo, S. Shu, Z. Liu, Y. Liu, J. Kong, E. Ma, Y. Cao, R.-S. Liu, X. Chen. Nature Commun. **5**, 4312 (2014).
[6] B. Henderson, G.F. Imbusch. Optical spectroscopy of inorganic solids. Oxford University Press (2006).
[7] S. Adachi. ECS J. Solid State Sci. Technol. **9**, *1*, 016001 (2020).
[8] T. Senden, R.J.A. van Dijk-Moes, A. Meijerink. Light: Sci. Appl. **7**, 8 (2018).
[9] S. Adachi. ECS J. Solid State Sci. Technol. **10**, *2*, 026002 (2021).
[10] S. Adachi. ECS J. Solid State Sci. Technol. **11**, *3*, 036001 (2022).
[11] S. Adachi. ECS J. Solid State Sci. Technol. **10**, *12*, 128501 (2021).
[12] S. Adachi. ECS J. Solid State Sci. Technol. **10**, *7*, 076007 (2021).
[13] S. Yan. ECS J. Solid State Sci. Technol. **9**, *10*, 106004 (2020).
[14] T. Jansen, J. Gorobez, M. Kirm, M.G. Brik, S. Vielhauer, M. Oja, N.M. Khaidukov, V.N. Makhov, T. Jüstel. ECS J. Solid State Sci. Technol. **7**, *1*, R3086 (2017).
[15] Q. Zhang, X. Wang, X. Ding, Y. Wang. lnorg. Chem. **56**, *12*, 6990 (2017).
[16] S. Tian, B. Liu, L. Zhao, Z. Liu, X. Fan, L. Yang, Q. Min, H. Zhang, X. Yu, J. Qiu, X. Xu. J. Alloys Compd. **800**, 224 (2019).
[17] L. Zhang, L. Dong, Y. Xu, S. Yin, H. You. J. Lumin. **236**, 118084 (2021).
[18] D. Hou, H. Lin, Y. Zhang, J.-Y. Li, H. Li, J. Dong, Z. Lin, R. Huang. Inorg. Chem. Front. **8**, *9*, 2333 (2021).
[19] R.D. Shannon. Acta Crystallogr. A **32**, *5*, 751 (1976).
[20] S. Adachi. ECS J. Solid State Sci. Technol. **9**, *2*, 026003 (2020).
[21] S. Shionoya, W.M. Yen, H. Yamamoto. In: Fundamentals of luminescence / Ed. E. Nakazawa. CRC Press, Boca Raton, USA (2007).